



OPEN

# Micro-battery Development for Juvenile Salmon Acoustic Telemetry System Applications

SUBJECT AREAS:

BATTERIES

CHEMICAL ENGINEERING

Received  
24 September 2013Accepted  
24 December 2013Published  
21 January 2014Correspondence and  
requests for materials  
should be addressed to  
Z.D.D. (zhiquan.deng@  
pnnl.gov) or J.X. (jie.  
xiao@pnnl.gov)

Honghao Chen, Samuel Cartmell, Qiang Wang, Terence Lozano, Z. Daniel Deng, Huidong Li, Xilin Chen, Yong Yuan, Mark E. Gross, Thomas J. Carlson &amp; Jie Xiao

Energy and Environment Directorate, Pacific Northwest National Laboratory, 902 Battelle Blvd, Richland, WA 99352, US.

The Endangered Species Act requires actions that improve the passage and survival rates for migrating salmonoids and other fish species that sustain injury and mortality when passing through hydroelectric dams. To develop a low-cost revolutionary acoustic transmitter that may be injected instead of surgically implanted into the fish, one major challenge that needs to be addressed is the micro-battery power source. This work focuses on the design and fabrication of micro-batteries for injectable fish tags. High pulse current and required service life have both been achieved as well as doubling the gravimetric energy density of the battery. The newly designed micro-batteries have intrinsically low impedance, leading to significantly improved electrochemical performances at low temperatures as compared with commercial SR416 batteries. Successful field trial by using the micro-battery powered transmitters injected into fish has been demonstrated, providing an exemplary model of transferring fundamental research into practical devices with controlled qualities.

The Juvenile Salmon Acoustic Telemetry System (JSATS)<sup>1–3</sup> was developed by the U.S. Army Corps of Engineers, Portland District, to estimate the survival and observe the behavior of juvenile salmonoids passing through hydropower dams in the Federal Columbia River Power System located on the mainstream Columbia and Snake Rivers<sup>4,5</sup>. Acoustic micro-transmitters currently in use (Fig. 1a) are surgically implanted in test fish. The weight and volume of the transmitter needed to be reduced and the transmitter's dimensions and shape optimized for passage through the shaft of an injection needle in order to decrease the amount of handling required to implant transmitters, the effect of the tags on fish health and the cost of implantation, (Fig. 1b)<sup>6</sup>.

Currently, the primary batteries for the JSATS micro acoustic transmitters (Advanced Telemetry Systems, Inc., Isanti, MN, USA), are two 1.55-V silver oxide button cells (SR416), which comprise approximately 60% of total weight and 20% of total volume of the transmitter. Two stacked SR416s are necessary to supply the 3 V voltage required by the transmitter circuit. Reduction in the volume and weight of the battery is essential to achieve the goal of an injectable transmitter. In addition to size and weight concerns, new battery chemistries and packaging designs are necessary to improve both gravimetric and volumetric energy density and extend the lifespan of the battery to power the downsized transmitter.

Lithium chemistry has been selected to improve battery energy density because of the lightweight and highest negative potential of lithium. Various compounds are available as cathode materials in primary lithium batteries, such as  $\text{MnO}_2$ <sup>7–9</sup>,  $\text{I}_2$ <sup>10,11</sup>,  $\text{FeS}_2$ <sup>12,13</sup> or  $\text{SOCl}_2$ <sup>14,15</sup> *et al.* For the new JSATS transmitter, lithium/carbon fluoride (Li/CF<sub>x</sub>) batteries were chosen as the candidate to replace the current silver oxide cells because of their many advantages, including high power density, high average operating voltage, long shelf life, and wide operating temperature<sup>16–20</sup>. Theoretically, carbon monofluoride (CF<sub>x</sub> with x = 1) has a high capacity of 864 mAh/g<sup>20–22</sup>. Its practical energy density reaches up to 650 Wh/kg in an envelope cell design<sup>19</sup>, more than four times higher than that of SR416 (less than 150 Wh/kg, originated from Energizer)<sup>23</sup>. However, the operating voltage of a Li/CF<sub>x</sub> cell exhibits a delay accompanied by a significant polarization at high discharge rates, mainly because of the low electronic conductivity of CF<sub>x</sub><sup>16,24</sup>. Other issues also exist in the practical application of Li/CF<sub>x</sub> cells such as heat generation during the discharge process, which can be significant at elevated current densities<sup>25,26</sup>. To address those problems in a micro-battery employing Li/CF<sub>x</sub> chemistry, it is necessary to increase the electronic conductivity of the entire CF<sub>x</sub>/C electrode and minimize the internal resistance as well as the size of the cell<sup>27</sup>.

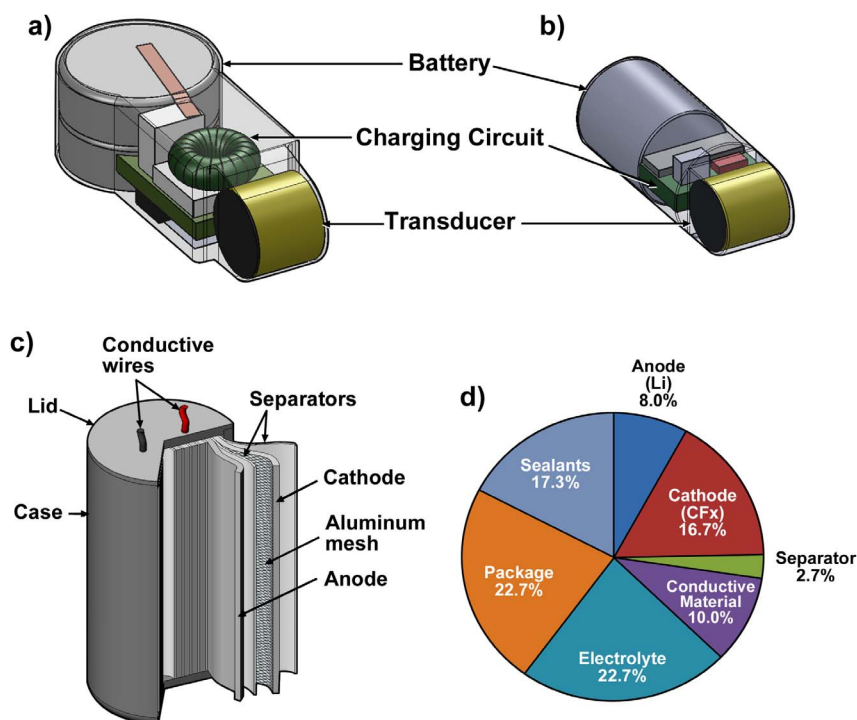


**Figure 1 | Acoustic transmitters.** (a) current JSATS transmitter design. (b) a newly proposed downsized design. (c) cross-sectional view. (d) weight distribution of PNNL-made MB306.

In this work, specifically designed micro-batteries (MB306) have been developed for the JSATS project. This work focuses on the design and evaluation of the micro-battery part while more detailed characterizations on the as-fabricated electronic devices will be reported later. Through appropriate lamination and fabrication process, cylindrical  $\text{CF}_x$ -based micro-batteries have been prepared in the lab readily for mass production. The changes in impedance, high discharge rate characteristics, and high power pulse properties of micro-batteries along with temperature influences on battery performance are discussed in detail.

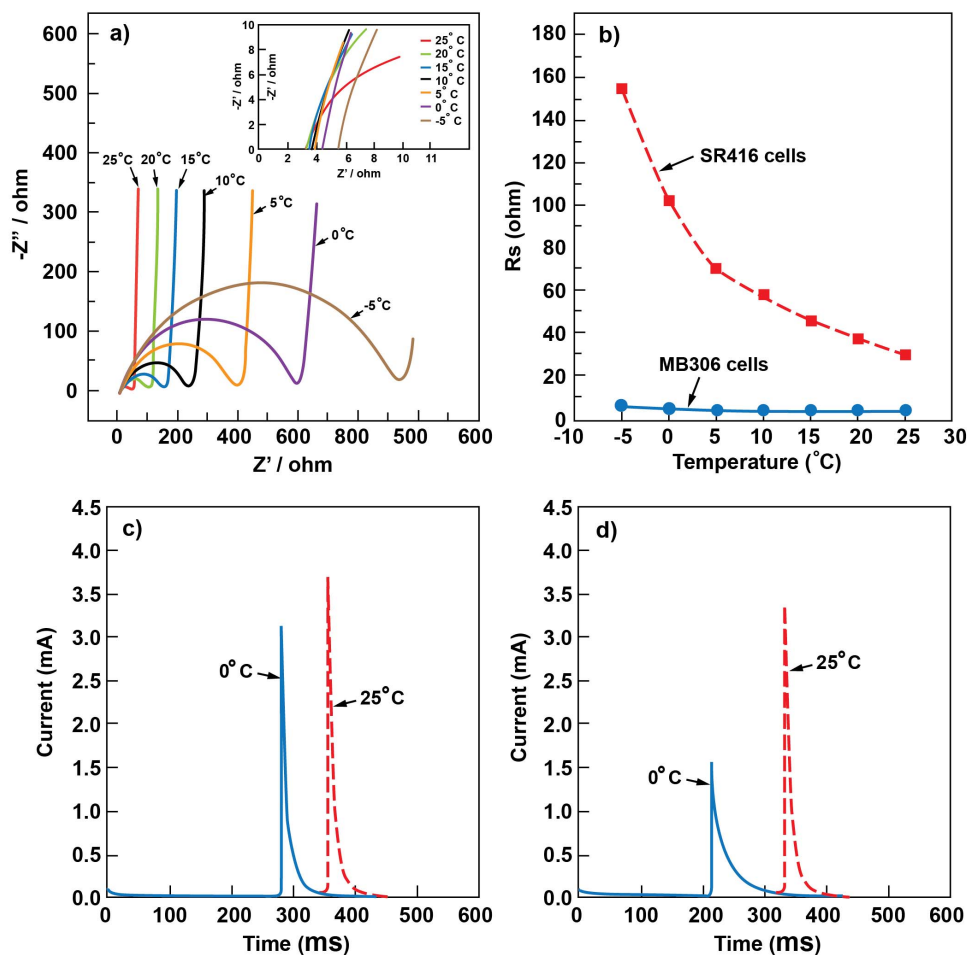
## Results

Fig. 1c illustrates the section structure of the micro-battery (MB306) developed in this work. The jelly-roll structure of MB306 cell enables the final cylindrical shape of the transmitter, which is critical for the injectable fish tag. Another advantage of this design is that the total capacity/energy can be increased conveniently by extending the length of the cell for other transmitters targeted to track bigger fishes. The weight distribution from each component of MB306 is plotted in Fig. 1d. The energy density of a battery usually goes down with decreasing battery dimension due to the increased weight from accessories. For example, weight contribution from cathode and anode together in MB306 cell is less than 25%. The parasitic weight from package, sealant, etc., accounts for a much larger portion of the total weight (Fig. 1d). A light packaging material with the necessary mechanical strength is helpful to further increase the micro-battery energy and worth exploration.

The lamination technique used in this work allows a high loading of  $\text{CF}_x$  on the limited electrode area ( $18 \text{ mg/cm}^2$ ) without significantly increasing the cell impedance, which is closely related with the battery performance especially at high pulse current. The usually observed voltage delay phenomena is removed during discharge under constant current (Fig. S1), even though the mass loading of  $\text{CF}_x$  in MB306 is five to ten times higher than that of the button cell results reported in literature. Fig. 2a shows the Nyquist plots for a fresh lab-made MB306 cell at different temperatures from  $-5^\circ\text{C}$  to

$25^\circ\text{C}$ . All the impedance spectra consist of a depressed semicircle in the medium- to high-frequency range and an inclined line in the low-frequency range. The depressed semicircle is attributed to the solid electrolyte interphase (SEI) film on the lithium anode in the high-frequency range and the charge transfer between electrolyte and active materials in the medium-frequency range. The near-vertical inclined line in the low-frequency range is due to the lack of lithium ion diffusion in active material because the irreversible reaction between the lithium ion and active material occurs on the surface of the active material,  $\text{CF}_x$ <sup>29</sup>. Every semicircle has two intercepts with the real axis (Fig. 2). The high-frequency intercept ( $R_S$ ) includes the resistance from the electrolyte, electrodes, and current collector/wires.  $R_S$  is the internal ohmic resistance of the battery. As discussed above, the medium-frequency intercept ( $R_t$ ) includes impedance arising from charge transfer, SEI film, and  $R_S$ .

Fig. 2b compares the response of  $R_S$  of MB306 and SR416 cells at different temperatures from  $-5^\circ\text{C}$  to  $25^\circ\text{C}$ . As the cold-blooded juvenile salmon migrate from freshwater into saltwater, the operating temperature of JSATS transmitters will vary between  $7^\circ\text{C}$  and  $22^\circ\text{C}$ , the temperature of the water through which the salmon are traveling. Therefore, we broaden the temperature range ( $-5^\circ\text{C}$  to  $25^\circ\text{C}$ ) to evaluate the micro-batteries to better understand their electrochemical performances under extreme conditions. Internal resistance of the MB306 cell was much lower than that of the SR416 button cells over the entire temperature range. This is mainly because the jellyroll design of the MB306 cell contains an increased total electrode area (approximately  $0.8 \text{ cm}^2$ ) for both the cathode and anode electrodes, ten times larger than that of the SR416 button cell (about  $9.6 \times 10^{-2} \text{ cm}^2$ ), which lowers the resistance arising from electrolyte and electrode interface. When the operating temperature decreased from  $25^\circ\text{C}$  to  $-5^\circ\text{C}$ , the conductivity of the electrolyte is reduced<sup>30</sup> as reflected by electrolyte viscosity measurements at different temperatures (see supporting information Fig. S2). However, the impedance of MB306 cell did not show big changes and always stayed at low values ( $5.5 \Omega$ ) suggesting that the ionic resistance of the organic electrolyte may only account for a small part of the total resistance.



**Figure 2 | Electrochemical behaviors.** (a) Comparison of the Nyquist impedance spectra of the MB306 cell at temperatures from  $-5^{\circ}\text{C}$  to  $25^{\circ}\text{C}$ . The inset of (a) shows a magnification of the impedance spectra in high frequency range. (b) Measured resistance of the MB306 cell and SR416 cells at temperatures ranging from  $-5^{\circ}\text{C}$  to  $25^{\circ}\text{C}$ . (c) Pulse current generated from the MB306 cell. (d) Pulse current generated from SR416 button cells at different temperatures.

In contrast, within the same temperature range, the impedance of the commercial SR416 button cells increased significantly from  $29\ \Omega$  to  $155\ \Omega$  (supporting information Fig. S3). In actual JSATS applications, this means that the transmitters powered by MB306 batteries will be more stable and efficient, especially at the current draw required for high transmission pulse rates, than those powered by SR416 button cells.

To further understand how impedance affects the function of the battery when JSATS transmitters are in fish migrating downriver, pulse current tests during discharge were performed to compare MB306 (Fig. 2c) and SR416 batteries (Fig. 2d). During each transmission, JSATS transmitter drew approximate 0.1 mJ of energy from a pair of SR416 batteries during a 100-ms-duration pulse at a transmission repetition interval of 3 s. At room temperature, both the MB306 and SR416 provide similar triangular current waveforms, satisfying the basic power requirement for the transmitters. When the temperature decreased to  $0^{\circ}\text{C}$ , the current waveform of MB306 changed slightly, indicating that a steady power was maintained to support the transmitter operation. In contrast, the current waveform of SR416 button cells became broader with reduced peak intensity. The height of the peak from SR416 decreased from 3.4 mA at  $25^{\circ}\text{C}$  to 1.53 mA at  $0^{\circ}\text{C}$ , which suggests that charging the transmitter circuit becomes more difficult (Fig. S4) at low temperatures and may even terminate the signal transmission due to the decreased energy supply.

The voltage profiles of both micro-batteries connected to JSATS transmitters were monitored between  $0^{\circ}\text{C}$  and  $30^{\circ}\text{C}$  (Fig. 3a). In this

condition, pulse current instead of constant current is supplied from the micro-batteries with 3 s intervals. Therefore, the voltage curves (green and blue lines) include both open circuit voltage (OCV) during the 3 s break as well as the operating voltage when pulse current is drawn from the battery. The open circuit voltage of MB306 is 2.71 V at  $30^{\circ}\text{C}$  and dropped slightly to 2.57 V at  $0^{\circ}\text{C}$ . The voltage change rate for the MB306 cell was approximately  $4.7\ \text{mV}/^{\circ}\text{C}$ , which is still within the acceptable voltage range required by the transmitter. Magnification of the operating voltage drop occurring in these two batteries upon a single transmission pulse at  $0^{\circ}\text{C}$  is plotted in the inset of Fig. 3a. The operating voltage drop (0.23 V) for SR416 button cells is more than twice that of the MB306, due to the greatly increased resistance at  $0^{\circ}\text{C}$  for the SR416 cells as discussed earlier in Fig. 2d. In real JSATS applications, overall voltage variation within the 3 s idle state of the MB306 is slightly larger than that for the SR416 cell. However, the MB306 cell supplies more stable voltage than the SR416 cell during transmission, which is more important for the practical use of JSATS transmitters.

The stable energy supply during transmission is further confirmed in Fig. 3b which compares the voltage variation and lifespan of both SR416 and MB306 tested by using real JSATS transmitters at room temperature. Both gravimetric and energy density have been largely improved in cylindrical MB306 when compared with SR416 (Table 1). The service life is therefore extended in MB306-powered transmitter, although two-stacked SR416 have to be used to meet the minimum voltage output required by the transmitter. The

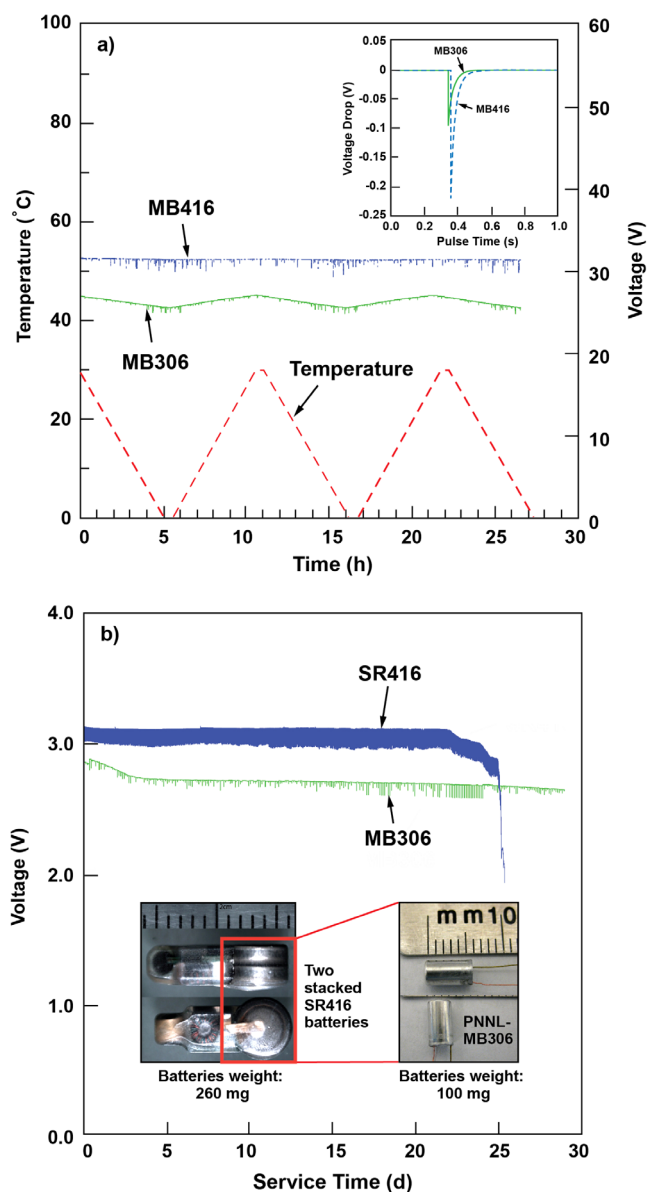


**Figure 3 | Micro-battery performance comparison.** (a) Voltage variation of SR416 and MB306 connected to JSATS transmitters as a function of temperature. Solid green line – MB306 cell; dotted blue line – SR416 button cells; dashed red line – ramp of temperature change ( $6^{\circ}\text{C}/\text{h}$ ). The insert of (a) compares the voltage drop of MB306 and SR416 during a pulse transmission at  $0^{\circ}\text{C}$ . (b) Voltage profile versus service time of SR416 and MB306. Both batteries were connected to a JSATS transmitter and operated at room temperature. The service life requirement of a power source driving a current JSATS transmitter is at least 20 days. The inset of (b) shows a photo of SR416 and MB306.

gravimetric energy of as-designed MB306 was more than twice that of the SR416. The most updated version of MB306 weighs only 70 mg thus further increasing the energy density of battery and reducing the burden on small fishes.

## Discussion

The two versions of batteries, SR416 and MB306, are shown in Fig. 3, in which the difference in size and shape can be clearly seen. The cylindrical high-energy density MB306 makes the tag injection for juvenile salmon feasible. In the field trial, seven hundred micro transmitters powered by MB306 were injected into the juvenile fish, which were then released into the Snake River of Washington State.

**Table 1 | Comparison of MB306 and SR416**

Typical Physical Parameters						
Battery Type	Dimensions		V	M	Energy Density	
	L	OD			Wh/kg	Wh/l
MB306	6.0	3.0	0.042	100	222	528
*SR416 $\times$ 2	3.2	4.8	0.058	260	100	443

\*Calculated from the SR416 datasheet of Energizer's silver oxide batteries.

Valuable data was successfully collected and used to evaluate the behavior and survival of the juvenile salmonids as they migrated through the Federal Columbia Power System. The major advantages of as-designed micro-battery include: 1) unique lamination technique allows high loading of active mass on aluminum mesh; 2) maximized electrode area in confined space minimizes the cell impedance and improves the rate performance of the micro-battery; 3) flexible cell design can be easily adapted into other types of micro-battery forms for various downsized flexible transmitters for many other species such as juvenile lamprey.

To the best of our knowledge, there is no micro-battery commercially available for this series of tags which may have a huge potential market in the near future. Practical gravimetric and volumetric energy densities have been remarkably improved, satisfying all requirements for powering JSATS transmitters. The newly designed micro-batteries have intrinsically much lower impedance than the commercial SR416 button cells, leading to significantly improved electrochemical performances over a wide temperature range. The micro-battery capability becomes a critical component to the development of current and future revolutionary injectable acoustic micro transmitter, which will result in significant reduction in cost of use, biological benefits for the tagged fish and provide information for the development of fish-friendly hydro systems internationally.

## Methods

Commercial carbon-coated  $\text{CF}_x$  (Advanced Research Chemicals, Inc) was used for cathode lamination without further treatment. 85 wt%  $\text{CF}_x$ , 10 wt% Super P carbon (Timcal), and 5 wt% of polytetrafluoroethylene (PTFE from DuPont) were mixed in isopropanol, followed by continuous stirring until the material forms a dough-like substance. The mixture was then laminated into a continuous film using a roller calendar and pressed onto Aluminum mesh to serve as the current collector. The laminated electrode was cut into different sizes to meet requirements. An enameled copper wire (0.13 mm OD) was attached to the aluminum mesh current collector. Lithium metal foil (from FMC) was used as the anode. All cells have a jellyroll design (Fig. 1c). Two layers of micro-porous polypropylene separator (Celgard Separator 2500) were used to tightly wrap the entire cell.

Once the dry battery was prepared, the bundled electrodes were inserted into the capsule case, which was filled with electrolyte (1 M LiPF<sub>6</sub> in ethylene carbonate/dimethyl carbonate (EC/DMC, volume ratio 1:1)). The lid was positioned on the case, and the cell was sealed with epoxy. Transmitter driving tests to evaluate the micro-batteries were performed by connecting the JSATS micro-acoustic transmitter directly to the micro-battery.

All of the prototype cells were assembled in an argon-filled glove box (MBraun Inc., Stratham, NH, USA). Evaluations were conducted at room temperature except for the temperature variation experiments, which were performed in a temperature chamber (Model TJR-A-WF4, Thermal Product Solutions, New Columbia, PA, USA). An Arbin tester (Model BT-2000, Arbin instruments Inc., College Station, TX, USA) was used for electrochemical tests. A CH Instruments (Model 650D, CH Instruments, Inc., Austin, TX, USA) electrochemical analyzer was used for the impedance analysis and current measurement. The impedance analysis was performed over a frequency range from 0.01 Hz to 100 kHz with an amplitude of 5 mV. Alternating current impedance is a powerful tool for measuring the impedance of batteries at different states<sup>28</sup>. The information obtained from impedance can be used to predict the performance and lifespan of a battery.

1. McMichael, G. A. *et al.* The Juvenile Salmon Acoustic Telemetry System; A New Tool. *Fisheries* **35**, 9–22 (2010).





2. Weiland, M. A. *et al.* A Cabled Acoustic Telemetry System for Detecting and Tracking Juvenile Salmon. Part 1: Engineering Design and Instrumentation. *Sensors-Basel* **11**, 5645–5660 (2011).
3. Deng, Z. D. *et al.* A Cabled Acoustic Telemetry System for Detecting and Tracking Juvenile Salmon: Part 2. Three-Dimensional Tracking and Passage Outcomes. *Sensors-Basel* **11**, 5661–5676 (2011).
4. Service, R. F. Will Busting Dams Boost Salmon? *Science* **334**, 888–892 (2011).
5. Service, R. F. Rejected Salmon Plan Could Bring Changes to U.S. Dams. *Science* **333**, 811–811 (2011).
6. Deng, Z. D. *et al.* Development of external and neutrally buoyant acoustic transmitters for juvenile salmon turbine passage evaluation. *Fisheries Research* **113**, 12 (2012).
7. Bowden, W. *et al.* New manganese dioxides for lithium batteries. *J. Power Sources* **165**, 609–615 (2007).
8. Park, M. S. & Yoon, W. Y. Characteristics of a Li/MnO<sub>2</sub> battery using a lithium powder anode at high-rate discharge. *J. Power Sources* **114**, 237–243 (2003).
9. Nishio, K., Yoshimura, S. & Saito, T. Discharge characteristics of manganese dioxide/lithium cells in various electrolyte solutions. *J. Power Source* **55**, 115–117 (1995).
10. Liang, C. C. & Holmes, C. F. Performance and reliability of the lithium/iodine battery. *J. Power Sources* **5**, 3–13 (1980).
11. Lin, M. L., Jin, Y. X., Zhang, Y. Z., Hou, Y. F. & Wang, S. D. Long-term discharge characteristics of lithium-iodine cells with an additive in poly(2-vinylpyridine) iodide. *J. Power Sources* **20**, 141–143 (1987).
12. Yang, S.-H. & Horn, Q. C. Chemical, structural and electrochemical comparison of natural and synthetic FeS<sub>2</sub> pyrite in lithium cells. *Electrochim. Acta* **46**, 2613–2621 (2001).
13. Iwakura, C., Isobe, N. & Tamura, H. Preparation of iron disulfide and its use for lithium batteries. *Electrochim. Acta* **28**, 269–275 (1983).
14. Iwamaru, T. & Uetani, Y. Characteristics of a lithium-thionyl chloride battery as a memory back-up power source. *J. Power Sources* **20**, 47–52 (1987).
15. Boyle, G. H. & Goebel, F. Development and characterization of a high capacity lithium/thionyl chloride battery. *J. Power Sources* **54**, 186–191 (1995).
16. Yazami, R. *et al.* Fluorinated carbon nanofibres for high energy and high power densities primary lithium batteries. *Electrochem. Commun.* **9**, 1850–1855 (2007).
17. Nagasubramanian, G. Fabrication and Testing Capabilities for 18650 Li/(CF<sub>x</sub>)<sub>n</sub> Cells. *Int. J. Electrochem. Sc.* **2**, 913–922 (2007).
18. Groult, H. *et al.* Improvements of the electrochemical features of graphite fluorides in primary lithium battery by electrodeposition of polypyrrole. *Electrochem. Commun.* **13**, 1074–1076 (2011).
19. Ritchie, A. G. *et al.* Further development of lithium/polycarbon monofluoride envelope cells. *J. Power Sources* **96**, 180–183 (2001).
20. Zhang, Q., D'Astorg, S., Xiao, P., Zhang, X. & Lu, L. Carbon-coated fluorinated graphite for high energy and high power densities primary lithium batteries. *J. Power Sources* **195**, 2914–2917 (2010).
21. Lam, P. & Yazami, R. Physical characteristics and rate performance of (CF<sub>x</sub>)<sub>n</sub> (0.33 < x < 0.66) in lithium batteries. *J. Power Sources* **153**, 354–359 (2006).
22. Zhang, S. S., Foster, D. & Read, J. Enhancement of discharge performance of Li/CF<sub>x</sub> cell by thermal treatment of CF<sub>x</sub> cathode material. *J. Power Sources* **188**, 601–605 (2009).
23. Energizer, [http://data.energizer.com/Europe/content/Batteries/silver\\_oxide.html](http://data.energizer.com/Europe/content/Batteries/silver_oxide.html).
24. Zhang, S. S., Foster, D. & Read, J. Carbothermal treatment for the improved discharge performance of primary Li/CF<sub>x</sub> battery. *J. Power Sources* **191**, 648–652 (2009).
25. Read, J., Collins, E., Piekarski, B. & Zhang, S. LiF Formation and Cathode Swelling in the Li/CF<sub>x</sub> Battery. *J. Electrochem. Soc.* **158**, A504–A510 (2011).
26. Zhang, S. S., Foster, D., Wolfenstine, D. & Read, J. Electrochemical characteristic and discharge mechanism of a primary Li/CF<sub>x</sub> cell. *J. Power Sources* **187**, 233–237 (2009).
27. Meduri, P. *et al.* Hybrid CF<sub>x</sub>-Ag<sub>2</sub>V<sub>4</sub>O<sub>11</sub> as a high-energy, power density cathode for application in an underwater acoustic microtransmitter. *Electrochem. Commun.* **13**, 1344–1348 (2011).
28. Seki, S. *et al.* AC Impedance Study of High-Power Lithium-Ion Secondary Batteries—Effect of Battery Size. *J. Electrochem. Soc.* **158**, A163–A166 (2011).
29. Levi, M. D. & Aurbach, D. Simultaneous Measurements and Modeling of the Electrochemical Impedance and the Cyclic Voltammetric Characteristics of Graphite Electrodes Doped with Lithium. *J. Phys. Chem. B* **101**, 4630–4640 (1997).
30. Chagnès, A., Carre, B., Willmann, P. & Lemordant, D. Modeling viscosity and conductivity of lithium salts in g-butylrolactone. *J. Power Sources* **109**, 203–213 (2002).

## Acknowledgments

The work described in this article was funded by the U.S. Army Corps of Engineers, Portland District. Brad Eppard is the technical lead for the USACE, and we greatly appreciate his leadership and support of this research. The authors are also grateful to many staff of the Pacific Northwest National Laboratory for their technical help—including Tylor Abel, Duane Balvage, Andrea Currie, Jayson Martinez, Praveen Meduri, Mitchell Myjak and Jinshan Xu. The study was conducted at PNNL, operated in Richland, Washington, by Battelle for the U.S. Department of Energy.

## Author contributions

H. Chen, Z. Deng and J. Xiao designed the micro-battery and analyzed the data, H. Chen, S. Cartmell, Q. Wang and T. Lozano assembled the cells and did the tests. H. Li and Y. Yuan tested micro-battery by using the fish tags. X. Chen analyzed the impedance data. M. Gross and T. Carlson involved in the results discussion and manuscript preparation.

## Additional information

Supplementary information accompanies this paper at <http://www.nature.com/scientificreports>

**Competing financial interests:** The authors declare no competing financial interests.

**How to cite this article:** Chen, H.H. *et al.* Micro-battery Development for Juvenile Salmon Acoustic Telemetry System Applications. *Sci. Rep.* **4**, 3790; DOI:10.1038/srep03790 (2014).



This work is licensed under a Creative Commons Attribution-NonCommercial-NoDerivs 3.0 Unported license. To view a copy of this license, visit <http://creativecommons.org/licenses/by-nc-nd/3.0>